The switching dynamics of the bacterial flagellar motor
Supporting Information
Siebe B. van Albada, Sorin Tănase-Nicola and Pieter Rein ten Wolde

Contents

In this *Supporting information* we provide background information on our model of the bacterial flagellar motor. We also derive the analytical solution of our coarse-grained model of the switching dynamics and explain the hybrid stochastic algorithm used in the simulations.

I. THE MODEL OF THE BACTERIAL FLAGELLAR MOTOR

A. Stator-Rotor interaction

The model for the stator-rotor interaction is discussed in the sections *The stator-rotor interaction* and *The rotor switching dynamics* of the main text. The model is based on the model Oster and Blair and coworkers [1, 2] and Meacci and Tu [3], but extended to include the conformational transitions of the rotor protein complex. Here, we discuss aspects of the model that are not discussed in the main text. But, for completeness, we also give the main equations already presented in the main text.

In our model, each stator-rotor interaction is described by 4 energy surfaces, $U_{s_j}^r$, with the subscript $s_j = 0, 1$ denoting the conformational state of stator protein j and the supersript $r = 0, 1$ denoting the conformational state of the rotor (clockwise or counterclockwise). The stator-rotor interaction potentials are periodic saw-tooth potentials. The 2 surfaces corresponding to the two conformatinal states of the stator protein are equal except for a shift of half a period, while the 2 surfaces corresponding to the conformatinal states of the rotor are each other's mirror image plus a shift. We assume that the stator proteins are fixed by the peptidoglycan layer and that only the rotor complex moves. The equation-of-motion of the rotor is then given by

$$\gamma_{\mathrm{R}} \frac{d\theta_{\mathrm{R}}}{dt} = -\sum_{j=1}^{N_{\mathrm{S}}} \frac{\partial U_{s_j}^r(\theta_j)}{\partial \theta_{\mathrm{R}}} - F_{\mathrm{L}} + \eta_{\mathrm{R}}(t). \tag{1}$$

Here, γ_{R} is the friction coefficient of the rotor; $U_{s_j}^r(\theta_j)$ is the free-energy surface shown in the Box of the main text, where $\theta_j = \theta_{\mathrm{R}} - \theta_{\mathrm{S}_j}$, with θ_{R} the rotor rotation angle and θ_{S_j} the fixed angle of stator protein j; $\eta_{\mathrm{R}}(t)$ is a Gaussian white noise term of magnitude $\sqrt{2k_{\mathrm{B}}T\gamma_{\mathrm{R}}}$; N_{S} is the number of stator proteins. The torque F_{L} denotes the external load. Its dynamics is given by

$$\gamma_{\mathrm{L}} \frac{d\theta_{\mathrm{L}}}{dt} = F_{\mathrm{L}}(\theta_{\mathrm{R}} - \theta_{\mathrm{L}}) + \eta_{\mathrm{L}}(t), \tag{2}$$

where γ_{L} is the drag coefficient of the load and η_{L} is a Gaussian white noise term of magnitude $\sqrt{2k_{\mathrm{B}}T\gamma_{\mathrm{L}}}$. While for describing the torque-speed relation it can be assumed that the load is coupled to the rotor via either an infinitely stiff spring or a spring of large, but finite stiffness [3], a more refined model is needed for describing the switching dynamics of a motor to which a flagellum is attached; this is described in the next section.
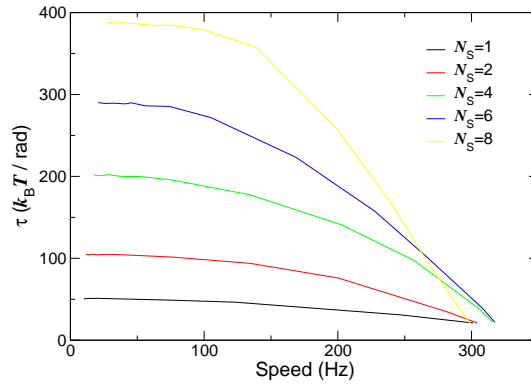
FIG. 1: The torque-speed relation as predicted by the model employed here, for different number of stators N_S. It is seen that the torque-speed relation exhibits the distinct knee at around 100 - 150 Hz and that the maximum speed is around 300 Hz, roughly independent of the number of stators. The parameters used in the simulations are shown in Table I.

The transition (or *hopping*) rate for a stator protein to go from one energy surface to another depends upon the rotatin angle in a manner that obeys detailed balance. It is given by

$$k^r_{s_j \to s'_j}(\theta_j) = k_0(\theta_j) \mathrm{MIN}\left[1, \exp[\Delta U^r_{s_j s'_j}(\theta_j)]\right], \ s, s'_j = 0, 1. \tag{3}$$

Here, $\Delta U^r_{s_j s'_j}(\theta_j) = U^r_{s'_j}(\theta_j) - U^r_{s_j}(\theta_j)$. Inspired by the observations of Meacci and Tu [3], the prefactor is given by $k_0(\theta_j) = k_-$ for $d_1 + m\delta < \theta_j < d_2 + m\delta$, where m is an integer and d_1 and d_2 are the minimum and maximum of the periodic potential with periodicity $\delta = 2\pi/26$; $k_0(\theta_j) = 0$ for $d_2 + m\delta < \theta_j < d_3 + m\delta$; $k_0(\theta_j) = k_+$ for $d_3 + m\delta < \theta_j < d_1 + (m+1)\delta d_1$. As shown by Meacci and Tu [3], the maximum speed becomes independent of the number of stators when $k_- > k_+$; this allows the "lagging" stators, which tend to drive the rotor backwards by exerting a negative torque on it, to catch up with the other stators that drive the rotor forward.

The rotor complex is modeled as an MWC model [4], which means that all the rotor proteins switch conformation in concert. This leads to the following expression for the instantaneous *switching* rate:

$$k^{r \to r'}(\{\theta_j\}) = \tilde{k}_0 \exp[\Delta U^{rr'}(\{\theta_j\})/2], \ r, r' = 0, 1, \tag{4}$$

where $\Delta U^{rr'}(\{\theta_j\}) = \sum_{j=1}^{N_S} \left(U^{r'}_{s_j}(\theta_j) - U^r_{s_j}(\theta_j)\right)$.

The parameters of the rotor-stator model, which were mostly taken from [1] and [3], are summarized in table I.

The torque-speed relation

Fig. 1 shows the torque-speed relation for different numbers of stators. It is seen that the torque-speed curve exhibits the characteristic "knee" at around $100 - 150$Hz and that the maximum speed is, to a good approximation, independent of the number of stators and equal to 300 Hz [5]. The maximum speed is important, since that, together with the change in winding angle of the filament upon a motor reversal, directly affects the position of the peak in the waiting-time distribution. For the results presented in this work, we assume that the number of stators is $N_S = 8$.

The mechanism of the load dependence of the switching rate

To understand how the average switching rate varies with the load, we note that the average switching rate is given by

$$k^{r \to r'}_{\mathrm{switch}} = \int d\theta_R P(\theta_R) k^{r \to r'}(\{\theta_j\}), \tag{5}$$

where $P(\theta_R)$ is the stationary distribution of the rotor's position and the instantaneous switching rate $k^{r \to r'}(\{\theta_j\})$ is given by Eq. 4. The instantaneous switching rate $k^{r \to r'}(\{\theta_j\})$ does not depend upon the load. However, increasing the load does change the stationary distribution $P(\theta_R)$ in such a way that the rotor is more often in positions where the driving force for switching, $\Delta U^{rr'}(\{\theta_j\})$, (see Eq. 4 above) becomes larger. This increases the average switching rate.

The mechanism that we propose differs fundamentally from that commonly used to explain the force dependence of processes such as protein unfolding and molecular dissociation [6]. The conceptual differences between the two

mechanisms are sketched in Fig. 2. In the conventional mechanism one assumes that the reaction coordinate can be described by a single order parameter, and that the load directly couples to that coordinate, changing the relative stability of the initial and final states, as well as the location and stability of the transition state separating them, as sketched in Fig. 2A. Applied to the switching of the bacterial flagellar motor, this mechanism would predict that the reaction coordinate is some order parameter that depends on the conformational state of the rotor, q_{switch} (Fig 2A), independent of the rotation angle of the rotor. In the mechanism that we propose, however, the propensity for the rotor to switch depends on the interactions with the stator proteins. Consequently, the reaction coordinate for switching depends not only on the coordinate describing the conformational state of the rotor protein complex, q_{switch}, but also on the rotation angle of the rotor θ_{R}, as shown in Fig. 2B. While the load may change the free-energy landscape in the direction describing the conformational state of the rotor, q_{rot}, in our model we assume that the load only couples to the rotation direction of the rotor; the load thus tilts the free-energy landscape in the rotation direction, θ_{R}, as denoted by the arrow in Fig. 2B, but not in the direction of the coordinate that describes the conformational state of the rotor, q_{switch}. However, the rate at which the rotor makes a conformational transition—the instantaneous switching rate—depends on the rotation angle θ_{R}, since that affects the free-energy difference with the transition state. Moreover, the stationary distribution of the rotation direction depends on the load, in such a way that increasing the load brings the rotor more often to positions θ_{R} where the free-energy barrier for switching is lower and the instantaneous switching rate thus higher. This is the principal mechanism that, according to our model, makes the effective switching rate $k_{\text{switch}}^{r \to r'}$, given by Eq. 5, sensitive to load and speed.

The effect of the potential shift on the load dependence of the switching rate

Fig. 3 shows the average switching rate as a function of the load, for different shifts between the CW and CCW surfaces. It is seen that for all shifts the switching rate increases with the load, although the nature of the increase depends on how much the CW surfaces are shifted with respect to the CCW surfaces. For small shifts, the switching rate increases exponentially with the motor torque, while for a shift of 0.5δ the increase is almost linear.

Recenty, Berg and coworkers measured the switching rate as a function of the motor torque in the zero-load regime [7]. The motor torque is defined as $\tau_{\text{m}} \equiv -\sum_{j=1}^{N_{\text{S}}} \left\langle \frac{\partial U_{s_j}^r(\theta_j)}{\partial \theta_{\text{R}}} \right\rangle$, and it is balanced by the load and the internal friction: $\tau_{\text{m}} = \gamma_{\text{L}}\omega + \gamma_{\text{R}}\omega \approx \gamma_{\text{L}}\omega$, where ω is the angular velocity. Indeed, Berg and coworkers assumed that the motor torque is equal to the load $\gamma_{\text{L}}\omega$, which means that their experimental data can be compared to the predictions of our model. Interestingly, they observed that the switching rate increases with the load [7], thus confirming a key prediction of our model. Moreover, their data suggests that the rate of increase is not exponential, but much weaker. Our model can reproduce this with a shift between the CW and CCW surfaces of 0.5δ (Fig. 3), not only when the linker that connects the load to the rotor is infinitely stiff as assumed here, but has a finite stiffness of $k_\theta = 1000 k_{\text{B}}T/\text{rad}^2$.

Eq. 5 makes it possible to understand how the increase of the switching rate with the load depends on the shift. For a shift of $\approx 0.1\delta$, the driving force $|\Delta U^{rr'}(\{\theta_{\text{R}}\})|$ increases linearly with the rotation angle over almost the whole range $0 < \theta_{\text{R}} < \delta$ (see Fig. 3A). Since the instantaneous switching rate depends exponentially on $\Delta U^{rr'}(\{\theta_{\text{R}}\})$, this

Parameter	Value	Description
δ	2π rad/26	Potential periodicity
ΔG	$20\ k_{\text{B}}T$	$\Delta G = 2e \times$ pmf
k_+	$13 \times 10^3\ \text{s}^{-1}$	Hopping prefactor positive torque
k_-	$19 \times 10^4\ \text{s}^{-1}$	Hopping prefactor negative torque
d_1	0.0	Position potential minium
d_2	$0.05\ \delta$	Position potential maximum
d_3	$0.15\ \delta$	Boundary hopping window
h	$14\ k_{\text{B}}T$	Height potential maximum
$F_{\text{M}} = -h/(\delta - d_2\delta)$	$61\ k_{\text{B}}T\ \text{rad}^{-1}$	Force motor during power stroke
γ_{M}	$0.01\ k_{\text{B}}T\text{s}\ \text{rad}^{-2}$	Friction coefficient motor
$\tilde{k}_0$	$0.05\ \text{s}^{-1}$	Switching prefactor
γ_{L}	$0.01 - 1.0 k_{\text{B}}T\ \text{s}\ \text{rad}^{-2}$	Friction coefficient load
k_θ	$1000 k_{\text{B}}T/\text{rad}^2$	Stiffness load-rotor linker torque-speed

TABLE I: Parameters for the rotor-stator model as used in the simulations (see also [1, 3]).
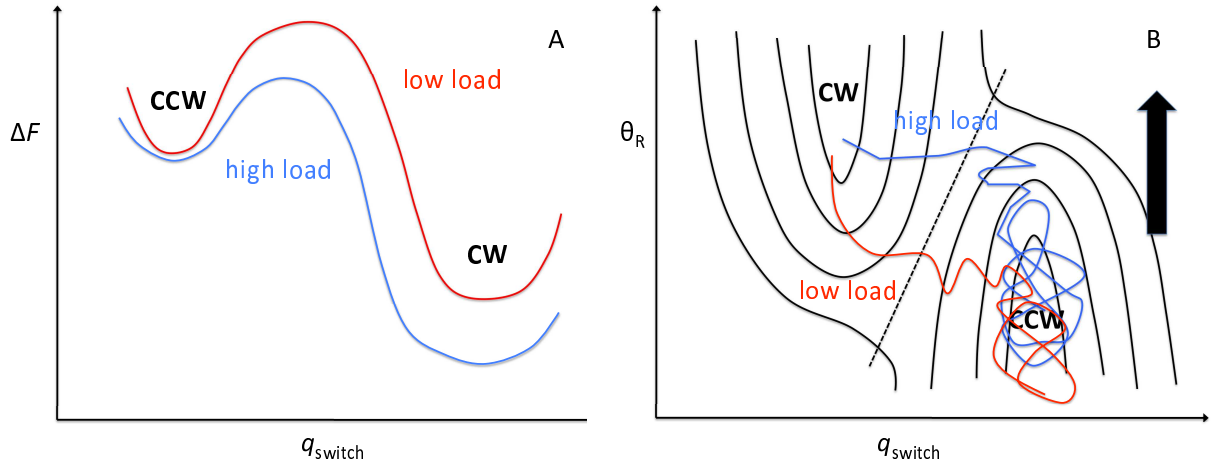
FIG. 2: A sketch of the conceptual differences between the conventional mechanism to explain the load dependence of the switching rate (A) and the mechanism that we propose (B). In the conventional mechanism (A), it is assumed that the progress of the switching process can be described by a single order parameter, q_{switch}, and that the load directly couples to that coordinate, thus changing the relative stability of the initial and final states, as well the transition state separating them. In particular, increasing the load lowers the free-energy difference ΔF between the initial state and the transition state, thus increasing the rate. In the scenario that we propose, the propensity for the rotor to switch depends on interactions with the stator proteins. Consequently, the reaction coordinate for the switching process depends on two order parameters (B). One describes the conformational state of the rotor, q_{switch}, and the other is the rotation angle of the rotor θ_{R}. The free-energy landscape depends on both order parameters, as illustrated in the contour plot of B, where the black solid lines denote contours of equal free energy. The load couples to the rotation direction θ_{R}, but not directly to the conformational state of the rotor, q_{switch}. Increasing the load thus tilts the free-energy landscape in the direction of θ_{R}, as denoted by the black solid arrow, but not in the direction of q_{switch}. However, the free-energy barrier for switching and hence the instantaneous switching rate depends on θ_{R}, and the stationary distribution of θ_{R} depends on the load. As a result, increasing the load brings the system more often to positions where the free-energy barrier for switching is lower and the instantaneous switching rate is higher. This is illustrated by the two trajectories in B, corresponding to a scenario where the load is low (red trajectory) and high (blue trajectory). It is seen that at high load (blue trajectory), the system is more often in positions where the free-energy barrier for crossing the transition-state surface, denoted by the dashed line, is lower, and the switching rate thus higher. A conformational transition of the stator corresponds to a discrete jump in the rotation angle θ_{R}.

explains why the effective switching rate increases drastically with the load when the shift is small (see Fig. 3B). However, for a shift of 0.5δ, the energy difference $|\Delta U^{rr'}(\{\theta_{\text{R}}\})|$ depends *non-monotonically* on the rotation angle θ_{R} over the range of angles that are of interest—it increases to reach a maximum at $\theta_{\text{R}} = 0.5\delta$, after which it first decreases before it rises again (Fig. 3A). The net result is a much weaker dependence of the average switching rate on the load.

Robustness of the switching mechanism

In our model, the characteristic switching time arises because of the interplay of two ingredients: 1) After a switching event, the load is initially low, but then rises to reach a plateau value; 2) rhe switching propensity increases with the load in the low-load regime. These two ingredients together create a switching-propensity that changes in a step-like fashion as a function of time, which is the origin of the characteristic switching time.

The first ingredient is a consequence of polymorphic transitions of the flagellum, which release elastic strain energy. These polymorphic transitions have not only been observed in pulling experiments on single flagella [8], but also in flagella of swimming bacteria during tumbles [9]. The first mechanism is thus a robust consequence of the elastic properties of flagellar filaments. It ensures that the plateau load τ_{max} as set by the balance of the drag force and the motor torque, is larger than the load τ_{min} at which the flagellum undergoes a polymorphic transition

The second ingredient—the switching propensity increases with the load in the low-load regime—arises from the interactions between the stator proteins and the rotor. How the switching rate increases with the load depends on the slope of the stator-rotor interaction potential, the shift between the CW and CCW energy surfaces, and the switching prefactor $\tilde{k}_0$. The slope of the stator-rotor interaction potential is very much dictated by the torque-speed relation, and can thus not be varied freely. The switching prefactor, however, is a free parameter that can be used to tune how strongly the switching rate varies with the load (Fig. 1 of the main text): the rate of increase is proportional to the magnitude of the switching prefactor. As discussed above, the nature of the increase also depends on the shift between the CW and CCW energy surfaces: while for a shift of 0.1δ the increase of the switching rate with the load
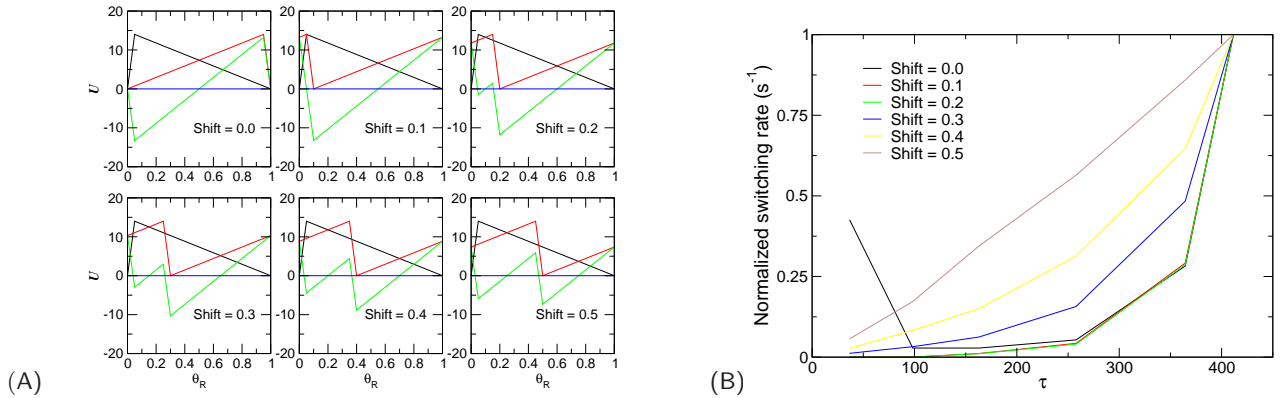
FIG. 3: (A) The CW (black line) and CCW (red line) energy surfaces, as well as the difference in energy between the two (green line), for different shifts. The rotation angle θ_R and the shifts are given in units of the period of the potential, $\delta = 2\pi/26$. The CW bias is 0.5. The driving force for switching from the CW state (black line) to the CCW state (red line) increases as the energy difference (green line) becomes more negative. Please note that when the shift is 0.1, the energy difference decreases almost monotonically with decreasing rotation angle θ_R; this explains why for a shift of 0.1 the switching rate increases strongly with the load (panel B). In contrast, when the shift is 0.5, as the rotation angle is decreased from 1, the energy difference first decreases, but then increases before it decreases again. This explains why for a shift of 0.5 the rate of increase of the switching rate with the load is rather weak (panel B). (B) The normalized average switching rate as a function of the load, for different shifts between the CW and CCW energy surfaces (see panel A). It is seen that the rate of increase decreases as the shift is increased. The initial drop in the switching rate as a function of the motor torque for a zero shift can be explained by noting that when the load is increased from zero and the average rotation angle decreases from unity (assuming that the motor runs in the CW direction, black line panel A), the energy difference between the CW and CCW surfaces initially increases (panel A). The flagellum dynamics has been integrated out; this corresponds to a conservative load, which is coupled to the rotor via an infinitely stiff spring [3].

is exponential, the increase for a shift of 0.5δ is fairly linear (Fig. 3). The question that arises is how sensitive the characteristic switching time is to the load dependence of the switching rate.

The *magnitude* of the increase of the switching rate k between the minimum load $\tau_{\min}$ and the maximum load $\tau_{\max}$, $\Delta k = k(\tau_{\max}) - k(\tau_{\min})$, is important for the switching dynamics. However, how the switching rate increases between $k(\tau_{\min})$ and $k(\tau_{\max})$, linearly or exponentially, is of minor importance. This is because polymorphic transitions make that after a switching event the load remains around a low value $\tau_{\min}$, until it *rapidly* rises to the plateau $\tau_{\max}$ when the flagellum has reached its final polymorphic form (see Fig. 3A of the main text).

To illustrate this we have analyzed the waiting-time distributions for a model in which the shift between the CW and CCW surfaces is 0.1δ. The results are shown in Fig. 4. It is seen that the waiting-time distributions have a marked peak, which means that there is a characteristic switching time [10]. The mechanism of the characteristic switching time that we propose is thus robust: any model in which the switching rate increases significantly with the load in the low-load regime, and in which the load initially remains low after a switching event, will give rise to a characteristic switching time.

A close examination of the waiting-time distribution reveals that the distribution for the CCW → CW transition is close to zero for small times $t < 0.2$s, even when the CW bias is 0.9. This is in contrast with the model presented in the main text, where the probability density becomes non-zero (see Fig.2A of main text). The difference is due to the fact that when the shift between the CW and CCW energy surface is 0.1δ, the switching rate at low torque is essentially zero, $k(\tau_{\min}) \approx 0$, while for a shift of 0.5δ, $k(\tau_{\min})$ has a non-zero value (see Fig. 3). The data of Korobkova *et al.* [11] suggests that the waiting-time distribution for the CCW → CW transition increases significantly with the CW bias for times $t < 0.2$s, supporting the model of the main text with a shift of 0.5δ. Our model predicts that the waiting-time distribution decays exponentially in this regime $t < 0.2$s (Fig.2A of the main text), which cannot be observed in the data of Korkobkova *et al.* because they used a sampling time of 0.1s. However, we would like to stress that this prediction is a result of the simplifying assumption of our model that the potential wells of the different polymorphic states of the flagellum are equal: if the torque to induce a polymorphic transition would increase as the flagellum approaches its final polymorphic form, then this exponential decay at early times would disappear [12]. The characteristic switching time would, however, remain, provided that $k(\tau_{\max}) > k(\tau_{\min})$ [12].

Finally, we show in Fig. 3B how the switching prefactor $\tilde{k}_0$ can be used to tune the waiting-time distributions. It is seen that when the kinetic prefactor is high, the waiting-time distribution has a strong peak. This is because a high switching prefactor leads to a large Δk, and this in turn means that the system tends to switch back before it reaches the plateau regime in which the switching propensity function is constant (See Fig.3B of the main text). In
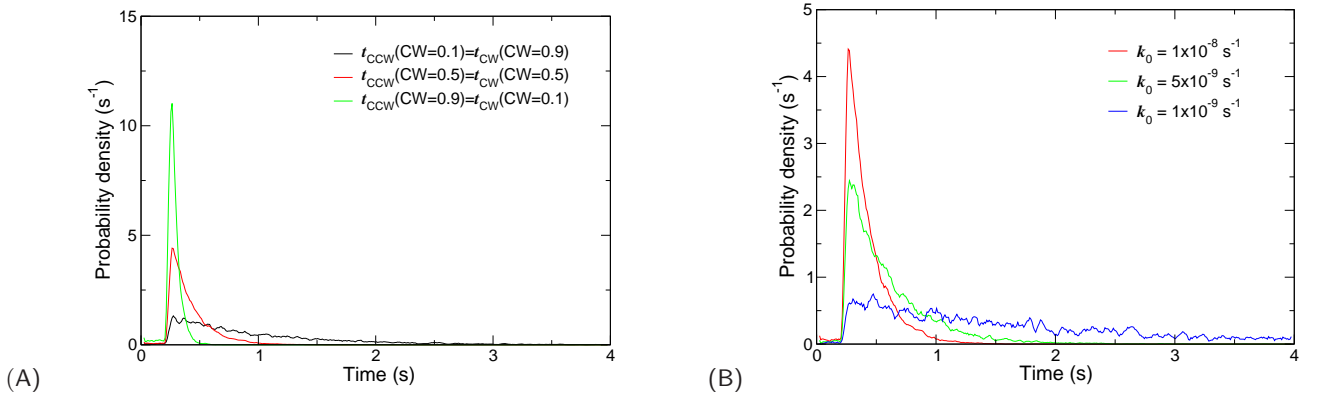
FIG. 4: (A) The waiting-time distributions for a model in which the shifts between the CW and CCW potentials is 0.1δ. The prefactor is $\tilde{k}_0 = 10^{-8}\mathrm{s}^{-1}$, while the other parameters are given in Table I. It is seen that the distributions have a marked peak, which means that there is a characteristic switching time. (B) The waiting-time distribution for the same system with a CW bias of 0.5, but with different switching prefactors $\tilde{k}_0$.

contrast, when the kinetic prefactor is small, Δk is small, and the system will enter the plateau regime in which the switching propensity is constant, leading to a long exponential tail of the waiting-time distribution.

B. The flagellar filament

We assume that the free energy of a flagellar filament in a given polymorphic state m is quadratic in the curvature κ and torsion τ:

$$U_m^{\mathrm{F}}(\tau, \kappa)/L = \frac{1}{2}EI(\kappa - \kappa_m)^2 + \frac{1}{2}\mu J(\tau - \tau_m)^2, \tag{6}$$

where L is the contour length, E and μ are the Young's and shear moduli, I and J are cross-sectional moments, and κ_m and τ_m are, respectively, the spontaneous curvature and torsion of the filament in state m. The curvature and torsion are functions of the height z and the winding angle θ:

$$\kappa(\theta, z) = \frac{\theta\sqrt{L^2 - z^2}}{L^2}, \tag{7}$$

$$\tau(\theta, z) = \frac{\theta z}{L^2}. \tag{8}$$

We assume that at each instant the length of the filament has relaxed to its steady state value $z_{\mathrm{eq}}(\theta)$, obtained as a solution of the equation $\frac{\partial U(\tau(\theta,z),\kappa(\theta,z))}{\partial z} = 0$. This allows us to elimate z and express the "torsional" energy as a function of the winding angle θ:

$$U_m^{\mathrm{T}}(\theta) = U_m^{\mathrm{F}}(\tau(\theta, z_{\mathrm{eq}}(\theta)), \kappa(\theta, z_{\mathrm{eq}}(\theta))), \tag{9}$$

The function $U_m^{\mathrm{F}}(\theta)$ is, in general, a complicated fonction of θ; nevertheless in the limit of equal bending and twisting stiffnesses ($EI = \mu J$) [8] the torsion potential corresponds to a linear elastic potential

$$U_m^{\mathrm{F}}(\theta) = \frac{1}{2}k_\theta(\theta - \theta_m)^2, \tag{10}$$

where $k_\theta = \frac{EI}{L}$ and $\theta_m = \frac{\sqrt{\kappa_m^2 + \tau_m^2}}{L}$. The eperimental data of Darnton and Berg [8] confirm that the approximation $EI \simeq \mu J$ is valid and therefore, locally, the potential energy guiding the dynamics of the twisting angle θ has a simple linear elasticity form with elastic constant $k_m \simeq 100$ pN nm/rad^2 (obtained from $EI = \mu J = 3.5$ pN μm^2 and $L = 7.6, 19.6$ μm as in [8]). As described in the main text, we assume that the potentiall wells are equally spaced, are of the same depth and have the same curvature. Clearly, these assumptions could be relaxed by allowing, $e.g.$, the normal state to be more stable and to have a higher stiffness.

Parameter	Value	Description
$\theta_m - \theta_{m-1}$	150δ	Spacing of wells
k_θ	$10k_\mathrm{B}T/\mathrm{rad}^2$	Stiffness
N	15	Number of wells.
$\check{k}_0$	$10^{-7}\mathrm{s}^{-1}$	Jumping prefactor

TABLE II: Parameters describing the flagellar filament.

Motivated by the observations of Darnton and Berg [8], we assume that the transition from one polymorphic state to another is an activated process, with a rate constant given by

$$k_{m \to m'}(\theta) = \check{k}_0 \exp[(U_m^\mathrm{F}(\theta) - U_{m'}^\mathrm{F}(\theta))/2]. \tag{11}$$

The equation-of-motion for the bead is then given by

$$\gamma_\mathrm{L} \frac{d\theta_\mathrm{L}}{dt} = -k_\theta(\theta_\mathrm{L} - \theta_\mathrm{R} - \theta_m) + \eta_\mathrm{L}(t), \tag{12}$$

where, as before, γ_L is the friction coefficient of the bead, and η_L is a Gaussian white noise term of magnitude $\sqrt{2k_\mathrm{B}T\gamma_\mathrm{L}}$.

The parameters of the model are given in table II.

II.   COARSE-GRAINED MODEL OF THE SWITCHING DYNAMICS

We model the switching dynamics as a memoryless two-state system with switching-time distributions $\psi_+(t)$ switching from CW to CCW and $\psi_-(t)$ for switching from CCW to CW:

$$\mathrm{CW} \underset{\psi_-(t)}{\overset{\psi_+(t)}{\rightleftarrows}} \mathrm{CCW} \tag{13}$$

Lack of memory means in this context that the probability to switch from one state depends only on the time since the transition to that state – the system forgets everything before the last transition.

The switching-time distribution is related to the switching rate or switching propensity (the switching probability per unit amount of time) $k_\alpha(t)$ as

$$\psi_\alpha(t) = k_\alpha(t)\mathrm{e}^{-\int_0^t k_\alpha(t')dt'}. \tag{14}$$

One important characteristic of the stochastic trajectory of the system is the correlation function $C(t)$ of the characteristic function $\chi(t)$:

$$C(t) = \langle \chi(t)\chi(0) \rangle - \langle \chi \rangle^2. \tag{15}$$

We take $\chi(t) = 1$ if the system is in the CW state and $\chi(t) = 0$ otherwise. From the ensemble of all possible trajectories only the ones that are in the CW state both at time zero and at time t contribute to the correlation function at time t. Therefore, one can write the correlation function as

$$C(t) = [P(\mathrm{CW}, t; \mathrm{CW}, 0) - P(\mathrm{CW}, \infty; \mathrm{CW}, 0)] P(\mathrm{CW}, \infty; \mathrm{CW}, 0), \tag{16}$$

where $P(\mathrm{CW}, t; \mathrm{CW}, 0)$ is the probability that a trajectory is in the CW state at time t given that it starts in that state at time zero. Using a well established result in the theory of (alternating) two-state, memoryless renewal processes (see [13], Chapter 7) one can express this quantity in the Laplace domain as:

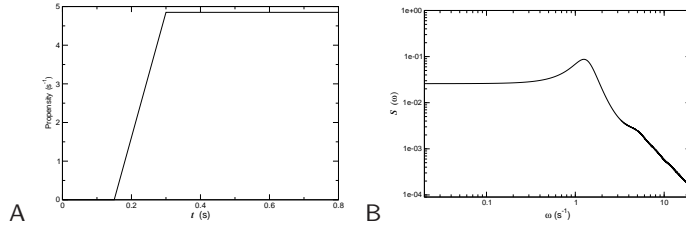$$\tilde{P}(z) = \frac{1}{z}\left(1 - \frac{G(z)}{zt_\mathrm{CW}}\right). \tag{17}$$

FIG. 5: A) A piecewise linear model of the switching-propensity function $k(t)$. B) Computed power spectrum $S(\omega)$.

Here, $\tilde{P}(z)$ is the Laplace transform of $P(\mathrm{CW}, t; \mathrm{CW}, 0)$,

$$\tilde{P}(z) = \int_0^\infty P(\mathrm{CW}, t; \mathrm{CW}, 0)\mathrm{e}^{-zt}dt, \tag{18}$$

$G(z)$ is a function that depends on the Laplace transformed switching-time distributions,

$$G(z) = \frac{(1 - \tilde{\psi}_+(z))(1 - \tilde{\psi}_-(z))}{(1 - \tilde{\psi}_-(z)\tilde{\psi}_+(z))}, \tag{19}$$

and t_{CW} is the average residence time in the CW state. The probability to be in the CW state is given by the average residence times as

$$P(\mathrm{CW}, \infty; \mathrm{CW}, 0) = \frac{t_{\mathrm{CW}}}{t_{\mathrm{CW}} + t_{\mathrm{CCW}}}. \tag{20}$$

Also, using the properties of the Laplace transform one has

$$\tilde{C}(z) = \frac{t_{\mathrm{CW}}}{t_{\mathrm{CW}} + t_{\mathrm{CCW}}} \left[\tilde{P}(z) - \frac{t_{\mathrm{CW}}}{z(t_{\mathrm{CW}} + t_{\mathrm{CCW}})} \right]. \tag{21}$$

Once we have the correlation function, we can compute the power spectrum using the formula

$$S(\omega) = 2 \int_0^\infty C(t) \cos \omega t = \tilde{C}(\mathrm{i}\omega) + \tilde{C}(-\mathrm{i}\omega), \tag{22}$$

such that

$$S(\omega) = \frac{1}{\omega^2(t_{\mathrm{CW}} + t_{\mathrm{CCW}})} \left[G(\mathrm{i}\omega) + G(-\mathrm{i}\omega) \right]. \tag{23}$$

In general, an analytical formula for the power spectrum $S(\omega)$ cannot be obtained for any arbitrary switching-propensity function $k_\alpha(t)$. Nevertheless, one can obtain an analytical formula for the power spectrum if the switching-propenstiy function is piecewise linear, as in Fig. 5A. Fig. 5B shows the power spectrum for a symmetric system, with switching-propensity functions in the forward and backward directions as shown in Fig. 5A. It is seen that this simple, non-Markovian two-state model can capture the main features of the power spectrum as measured by Korobkova *et al.*[11].

III. HYBRID STOCHASTIC ALGORITHM

The equations-of-motion for the rotor and the flagellum, Eqs. 1 and 10 of the main text, respectively, and Eqs. 1 and 12 above, are propagated via a Heun scheme [14].

The algorithm to determine when the next hopping, switching, or polymorphic transition will occur is essentially a kinetic Monte Carlo algorithm [15]. It is based on the observation that the *survival* probability $S(t)$, i.e. the probability that no hopping, switching or polymorphic transition has happened after a time t after the last event, is given by

$$S(t) = \exp\left(-a(t)\right), \tag{24}$$

where $a(t)$ is the cumulative total propensity function:

$$a(t) = \int_0^t dt' k_T(t'),$$ (25)

with $k_T(t)$ being the total propensity function as given by

$$k_T(t) = \sum_{j=1}^{N_S} k_{s_j \to s'_j}^r(\theta_j(t)) + k^{r \to r'}(\{\theta_j(t)\}) + k_{m \to m'}(\theta_L(t) - \theta_R(t) - \theta_m)).$$ (26)

In practice, right after a hopping, switching or polymorphic transition, a random number, ξ, between zero and one is drawn. The equations-of-motion of the rotor and the flagellum are then integrated together with the equation that describes the temporal evolution of $a(t)$:

$$\frac{da(t)}{dt} = k_T(t).$$ (27)

Integrating Eq. 27 since the last event leads to an estimate for $a(t) = \int_0^t dt' k_T(t')$. The next event then occurs after a time t since the last event when

$$a(t) > \log(1/\xi).$$ (28)

The event type α, where α is either a hopping, switching, or polymorphic transition, is subsequently chosen with a probability p_α as given by

$$p_\alpha(t) = k_\alpha(t)/k_T(t).$$ (29)

[1] J. Xing, F. Bai, R. Berry, and G. Oster, Proc Natl Acad Sci USA **103**, 1260 (2006), ISSN 0027-8424 (Print).
[2] S. Kojima and D. F. Blair, Biochemistry **40**, 13041 (2001).
[3] G. Meacci and Y. Tu, pnas **106**, 3746 (2009).
[4] J. Monod, J. Wyman, and J.-P. Changeux, J. Mol. Biol. **12**, 88 (1965).
[5] J. Yuan and H. C. Berg, Proc. Natl. Acad. Sci. USA **105**, 1182 (2008).
[6] J. Howard, *Mechanics of Motor Proteins and the Cytoskeleton* (Sinauer Associates, Inc., 2001).
[7] J. Yuan, K. A. Fahrner, and H. C. Berg, jmb **390**, 394 (2009).
[8] N. C. Darnton and H. C. Berg, Biophys J **92**, 2230 (2007 Mar 15), ISSN 0006-3495 (Print).
[9] N. C. Darnton, L. Turner, S. Rojevsky, and H. C. Berg, J Bacteriol **189**, 1756 (2007 Mar), ISSN 0021-9193 (Print).
[10] Y. Tu, Proc. Natl. Acad. Sci. USA **105**, 11737 (2008).
[11] E. A. Korobkova, T. Emonet, H. Park, and P. Cluzel, Phys. Rev. Lett. **96**, 058105 (2006).
[12] S. B. Van Albada, Ph.D. thesis, Vrije Universiteit Amsterdam (2008).
[13] D. R. Cox, *Renewal Theory* (Chapman and Halt, London, 1961).
[14] A. Greiner, S. W, and H. J, jsp **51**, 95 (1988).
[15] A. B. Bortz, M. H. Kalos, and J. L. Lebowitz, J. Comp. Phys. **17**, 10 (1975).